Time course of alterations in adult spinal motoneuron properties in the SOD1(G93A) mouse model of ALS

Seoan Huh[1], Charles J. Heckman[1,2,3], and Marin Manuel[1,4,§]

[1]Department of Physiology, [2]Department of Physical Medicine and Rehabilitation, and [3]Department of Physical Therapy and Human Movement Science, Northwestern University, Feinberg School of Medicine, Chicago, Illinois, USA. [4]Université de Paris, SPPIN - Saints-Pères Paris Institute for the Neurosciences, CNRS, Paris, France.

§ Corresponding author:

Marin MANUEL
SPPIN - Saints-Pères Paris Institute for the Neurosciences
Université de Paris, 45, rue des Saints-Pères, 75006 Paris, France
email: marin.manuel@neurobio.org

Author contribution

Conceptualization: S.H., C.J.H., and M.M.; Methodology: S.H., C.J.H., and M.M.; Investigation: S.H.; Formal analysis: S.H. and M.M.; Software: M.M.; Visualization: S.H. and M.M.; Writing - Original Draft: S.H.; Writing - Review & Editing: S.H., C.J.H., and M.M.; Funding Acquisition: C.J.H and M.M.; S.H., C.J.H., and M.M. approved the final version of this manuscript.

Number of pages: 33

Number of figures: 7 + 1 table

Number of words for abstract: 149

Number of words for Introduction: 514

Number of words for Discussion: 1860

Conflict of Interest

The authors have no conflict of interest to declare

Acknowledgements

This work was supported by NIH NINDS R01NS077863 and NINDS R01NS110953. S.H. was supported by a National Science Foundation Graduate Research Fellowship (NSF GRFP).

Abstract

Although ALS is an adult-onset neurodegenerative disease, motoneuron electrical properties are already altered during embryonic development. Motoneurons must therefore exhibit remarkable capacity for homeostatic regulation to maintain a normal motor output for most of the life of the patient. In the present paper, we demonstrate how maintaining homeostasis could come at a very high cost. We studied the excitability of spinal motoneurons from young adult SOD1(G93A) mice to end-stage. Initially homeostasis is highly successful in maintaining their overall excitability. This initial success, however, is achieved by pushing some cells far above the normal range of passive and active conductances. As the disease progresses, both passive and active conductances shrink below normal values in the surviving cells. This shrinkage may thus promote survival, implying the previously large values contribute to degeneration. These results support the hypothesis that motoneuronal homeostasis may be "hyper-vigilant" in ALS, and a source of accumulating stress.

Impact statement

During ALS, motoneurons attempt to maintain a normal motor output by altering their electrical properties, sometimes beyond the normal range, which may be causing long-lasting harm.

54 ## Introduction

55 ALS is a fatal neurodegenerative disorder characterized by progressive loss of
56 cortical and spinal motoneurons. Five to ten percent of the ALS cases are familial
57 (FALS), and ∼20% of the FALS cases are due to mutations in the Superoxide
58 Dismutase1 (SOD1) gene (Rosen et al., 1993). Studies in the mutant SOD1 (mSOD1)
59 mouse and other animal models have revealed that multiple cellular functions
60 become impaired as the disease progresses (Ilieva et al., 2009; Kanning et al., 2009;
61 Johnson and Heckman, 2010; Brownstone and Lancelin, 2018), implying that
62 homeostatic mechanisms are failing. Yet, the intrinsic excitability of neonatal and
63 young adult mSOD1 motoneurons undergoes a very potent and effective
64 homeostatic response to compensate an earlier surge in excitability in the
65 embryonic state (Kuo et al., 2004; van Zundert et al., 2008; Pieri et al., 2009; Martin
66 et al., 2013). The mechanisms of this successful homeostasis are however highly
67 unusual.

68 The standard measure of the net excitability of motoneurons is the relation
69 between frequency of firing of spikes and amplitude of injected current. This
70 frequency-current (F-I) function is determined by multiple ionic currents.
71 Remarkably, the successful F-I homeostasis in the neonatal state is achieved by
72 abnormal but compensatory increases in these currents. Persistent inward currents
73 (PICs), which are mediated by voltage gated Na^+ and Ca^{2+} channels, become
74 aberrantly large. On its own, this change would increase F-I gain, but it is
75 compensated by large increases in the leak currents that set the input conductance

76 of the cell. These abnormal changes show that F-I homeostasis during the neonatal
77 period is achieved via a compensatory mechanism. If, however, these compensatory
78 increases persist into the young adult state, then the continued distortions in input
79 conductances and PIC amplitudes could induce substantial stresses within the
80 motoneurons. In this scenario, the initial success in homeostatic regulation of net
81 excitability would be coupled to a severe cost, likely accelerating the onset of
82 degeneration. On the other hand, if homeostatic processes instead successfully
83 return input conductance and PIC values to normal ranges before the onset of
84 denervation, then homeostasis for the F-I function would reduce stress on the cell
85 and effects on subsequent degeneration would likely be small.

86 To investigate how homeostasis for excitability develops as the disease
87 progresses, we undertook the first *in vivo* voltage clamp studies of motoneurons in
88 the mouse and pursued these measurements across a wide range of ages, from P30
89 to P120. This age range spans the young adult period, the onset of denervation
90 period (～P50, Pun et al., 2006) and the development of overt symptoms (～P90).
91 We hypothesized that input conductance and PIC values would continue to grow in
92 the young adult state. Our results supported this hypothesis, revealing in fact a
93 continual increase in amplitude of these parameters, followed by a collapse, so that
94 motoneurons surviving beyond onset of overt symptoms (～P90) had aberrantly
95 small values of each. These results are consistent with the possibility that
96 homeostasis for excitability is not in fact weak but excessively strong and that this
97 overreaction contributes to subsequent degeneration (Mitchell and Lee, 2012).

Methods

Animals

This study was performed in strict accordance with the recommendations in the Guide for the Care and Use of Laboratory Animals of the National Institutes of Health. All of the animals were handled according to protocols approved by Northwestern University's institutional animal care and use committee (IACUC). All surgery was performed under sodium pentobarbital anesthesia, and every effort was made to minimize suffering. Because of the reproducible and stereotyped progression of symptoms, we chose to use mice overexpressing the human SOD1(G93A) gene, in which glycine has been substituted by alanine at residue 93 as a mouse model of ALS. All mice had a B6SJL background (Jackson Lab, Bar Harbor, ME). The transgene copy number was compared to a housekeeping gene at Transnetyx (Cordova, TN), and only mice with relative copy number >45 were used in this study. Control group consisted of non-transgenic littermates, with the same B6SJL background (WT). 33 animals of either sex were used in this study, and they were divided into different age groups for analysis: P30–60 (N=9 mice), P60–90 (N=12 mice), and P90–120 (N=12 mice).

In vivo preparation

Procedures were similar to those in our previous studies (Manuel and Heckman, 2011). Initially, atropine (0.2mg/kg) was administered subcutaneously to prevent salivation. Ten minutes later, anesthesia was initiated with an intraperitoneal injection of pentobarbital sodium (70 mg/kg) and maintained by intravenous infusion of supplemental doses of pentobarbital (6 mg/kg) mixed in perfusion

121 solution containing 4% glucose, 1% $NaHCO_3$, and 14% Plasmion. The trachea was
122 cannulated, allowing the mouse to be artificially ventilated with 100% O_2. The end-
123 tidal PCO_2 was continuously monitored and maintained around 4% by adjusting
124 ventilator parameters including respiratory rate around 120–150 bpm and tidal
125 volume around 0.09–0.23 mL. The hind limb muscles were then dissected; biceps
126 femoris was removed to expose the sciatic nerve, which was thereafter placed over
127 a stimulating electrode. A laminectomy was performed at T13–L1 level, and L3–L4
128 spinal segments were exposed. To prevent the spinal cord from dehydration, a
129 custom made bath was affixed using silicone elastomer and covered with mineral
130 oil. To locate the motoneurons of interest, the sciatic nerve was stimulated at
131 intensity 1.8× threshold for the apparition of an afferent volley.

132 **Electrophysiology**

133 Intracellular recordings of spinal motoneurons were performed by impaling them
134 with glass micropipette electrodes filled with 3M KCl with resistance of 8–15 MΩ.
135 Motoneurons were identified by the presence of antidromic action potential from
136 stimulation of the sciatic nerve. Cells with unstable resting membrane potential
137 (RMP) or with RMP more depolarized than −50mV were excluded from analysis.

138 PICs were recorded in discontinuous voltage clamp mode, with switching rates of
139 6–8 kHz. Clamp feedback gain was between 0.3 and 1.5. In addition to the feedback
140 gain from Axoclamp amplifier, an additional low-frequency feedback loop with a
141 gain of 11 and a cutoff of −3 dB at 0.3 kHz was used to improve voltage control in
142 such large cells as motoneurons (Lee and Heckman, 1998). Outputs were observed

143 at all times to assure reasonable settling of the electrode. To record PICs, a slow
144 triangular voltage ramp (−80 to −40 mV) was applied (Lee and Heckman, 1998).
145 Leak current was determined by fitting a regression line through the subthreshold
146 region of the I-V function. Then, this leak was subtracted from the total function to
147 determine the PIC amplitude (measured both on the ascending and descending part
148 of the ramp). In addition, the voltage at which the PIC was maximal on each part of
149 the ramp was recorded (PIC peak voltage), as well as the voltage at which the
150 current trace deviated from the leak current (PIC onset voltage) on the ascending
151 ramp, and joined back the leak trace on the descending ramp (PIC end voltage).
152 Input conductance was estimated as the slope of the leak current.

153 To assess intrinsic properties of the motoneuron in current clamp mode, we
154 measured the frequency-current (F-I) relationship of action potential firing. The F-I
155 relationship was determined based on the firing produced by a triangular current
156 injection. The interspike frequency was then plotted against the intensity of the
157 injected current. All these measurements were carried out in the discontinuous
158 current clamp mode of the Axoclamp 2A amplifier, with switching rates of 6–8 kHz.
159 Mouse motoneurons possess two regimes of firing: a sub-primary range of firing,
160 followed by a linear primary range (Manuel et al., 2009; Manuel and Heckman,
161 2011). The "gain" of the F-I relationship was determined by fitting a regression line
162 over the linear primary range (separately on the ascending and descending phase of
163 the ramp). The other parameters measured in the F-I relationship were: the current
164 at which the first action potential (AP) fires on the ascending ramp (recruitment
165 current). the current at which the last AP fires on the descending ramp (current at

166 de-recruitment); the voltage threshold for spiking, which was determined as the
167 voltage where the slope of the membrane voltage reaches 10mV/s before the first
168 AP (Sekerli et al., 2004); the current and firing frequency at the transition between
169 the sub-primary and primary ranges (Manuel and Heckman, 2011).

170 ## Data analysis

171 Recordings were acquired and analyzed using Spike2 v.7 (CED, Cambridge, UK).
172 Data were collected and analyzed using Pandas v.1.0.0 (McKinney, 2011), SciPy
173 Python v.1.4.1 (Virtanen et al., 2020) and DABEST v.0.3.0 (Ho et al., 2019). Figures
174 were generated using matplotlib v.3.1.3 (Hunter, 2007) and seaborn v.0.10.0
175 (Waskom et al., 2020).

176 ## Statistical analysis

177 All data are reported as mean ± standard deviation with their respective sample
178 size. No test was performed to detect outliers, and no data points were excluded
179 from analysis. When comparing between WT and mSOD1 samples, we focus on
180 estimation statistics that rely on effect sizes and confidence intervals (95%CI),
181 rather than null hypothesis significance testing, as recommended by several
182 scientific societies and editorial boards (Bernard, 2019; Makin and Orban de Xivry,
183 2019; Wasserstein et al., 2019; Michel et al., 2020). Unless otherwise specified, effect
184 sizes are reported as difference of means and Hedges' g (Hedges, 2016), as
185 calculated using DABEST v.0.3.0. (Ho et al., 2019). Where appropriate, data are
186 presented as Cumming plots (Cumming, 2012) generated using DABEST. In these
187 plots, the raw data are plotted as swarms of points. In addition, the mean ± standard

deviation of each group is plotted as a notched line immediately to the right of each group. The effect size and bootstrapped 95% CIs are plotted on a separate axes beneath the raw data. Confidence intervals were bias-corrected and accelerated, and are displayed with the bootstrap distribution of the mean; resampling was performed 5000 times (Ho et al., 2019). Welch's *t*-test (Welch, 1947) results are provided for information only.

Results

Motoneurons from young adult mutant mice have overly large PICs

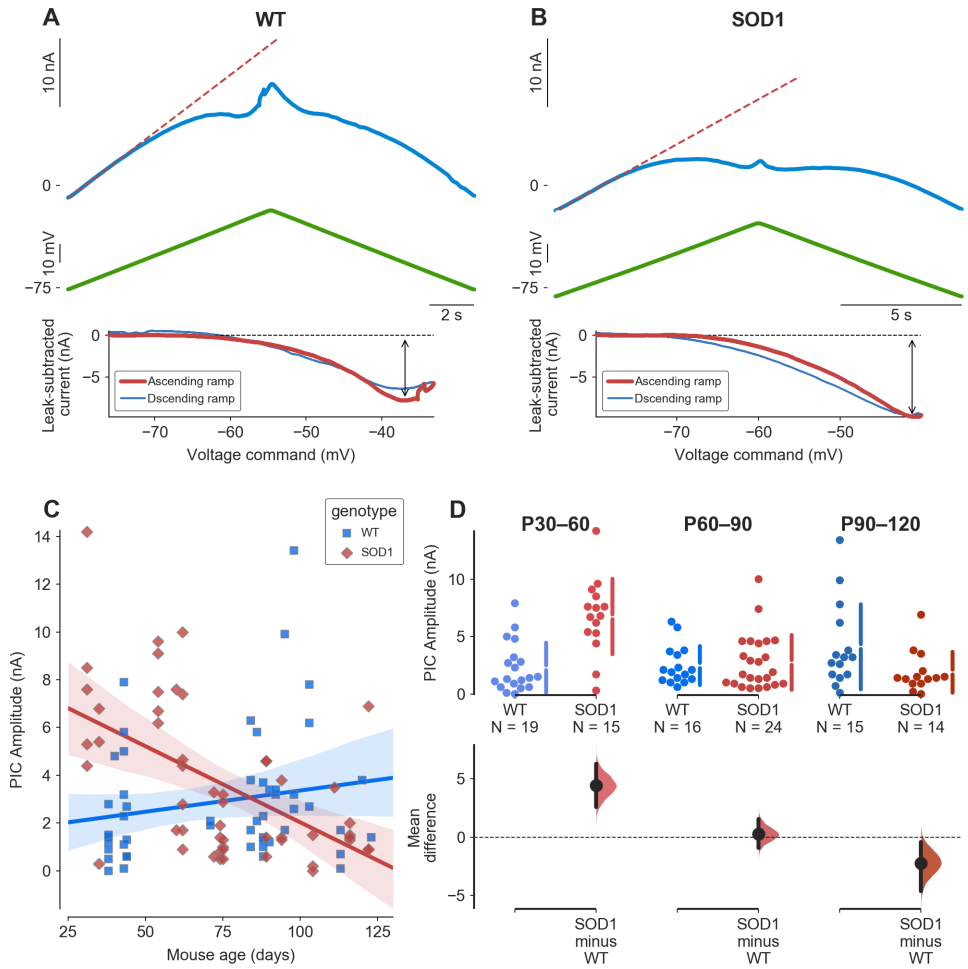

Figure 1: PIC amplitude is larger is young adult mSOD1 mice
A. Example of a PIC recording from a P43 WT mouse. Top trace: recorded current, bottom trace: voltage command. The red dashed line shows the leak current estimated by fitting a straight line around the point of zero current, and which is used to measure the input conductance of the cell. Below is a plot of the leak-subtracted current vs. the voltage command color coded for the ascending phase (thick red line) and the descending phase (thin blue line). The amplitude of the PIC is measured at the point indicated by the double arrow. Note that, in this example, a breakaway spike was filtered out. B. Example of a PIC recording from a P62 mSOD1 mouse. Same organization as in A. C. Plot of the amplitude of the PICs (in nA) vs. the age of the mouse in WT (blue square) and mSOD1 mice (red diamonds). The solid

lines correspond to the linear regression lines with 95% confidence intervals (shaded areas). Pearson correlation coefficients & 95%CI, WT: r=0.18 [−0.10–0.44] (p=0.2), mSOD1: r=−0.54 [−0.70–−0.31] (p=3.4e−5). D. Breakdown of the difference in PIC amplitude between WT and mSOD1 animals by age groups. P30–60 WT: 2.30±2.17nA, N=19 vs. mSOD1: 6.73±3.28nA, N=15; g=1.59 95%CI[0.63–2.45]; t(32)=−4.50, p=0.00016. P60–90 WT: 2.47±1.69nA, N=16 vs. mSOD1: 2.75±2.40nA, N=24; g=0.12 95%CI[−0.53–0.65]; t(38)=−0.42, p=0.67. P90–120 WT: 4.12±3.69nA, N=15 vs. mSOD1: 1.90±1.78nA, N=14; g=−0.74 95%CI[−1.26–0.01]; t(27)=2.08, p=0.05.

We set out to measure persistent inward currents (PICs) in 103 motoneurons from SOD1(G93A) mice (mSOD1), and their non-transgenic (WT) littermate, aged between 31 and 123 days old. PICs were measured in response to a slow (5 mV/s) ramp in voltage-clamp mode. The amplitude of the PIC was measured on the leak-subtracted trace at the point where the downward deflection of the trace was maximal (see Figure 1). In WT animals, the PIC amplitude remained roughly steady during the age period studied (Figure 1C). However, in mSOD1 motoneurons, PIC amplitudes decreased strikingly over time (slope=−0.45 nA/week, r=−0.54 95%CI[−0.70–−0.31], p=3.4e-5). When broken down by age groups (Figure 1D), our results shows that, in the young adult stage (P30–60), when animals are pre-symptomatic and neuromuscular-junction denervation is just starting, SOD1 mutation lead to an almost 3× increase in PIC amplitudes compared to WT motoneurons. This increase appears to be a continuation of the trend observed in neonates, where PICs were already increased ∼2-fold compared to controls (Quinlan et al., 2011). In the presymptomatic group (P60–90), however, this effect became negligible despite the fact that substantial denervation is already underway. At symptomatic stages (P90–120), the trend seen in young animals is reversed: PICs

234 are much smaller in mSOD1 motoneurons compared to WT motoneurons. Similar
235 results could be observed on the PIC amplitudes measured on the descending ramp
236 (Table 1).

237 In addition to its effect on PIC amplitude, SOD1 mutation also affected the voltage
238 at which PICs are recruited. The "PIC onset voltage", measured as the voltage at the
239 point where the leak-subtracted motoneuron I-V curve initially begins to curve
240 downward, was hyperpolarized by 10 mV in young mSOD1 mice compared to WT
241 controls (WT: −58.03±6.35mV, N=19 vs. mSOD1: −69.41±5.71mV, N=15; g=−1.83
242 95%CI[−2.64−−0.78]; t(32)=5.49, p=5.1e−06). The SOD1 mutation had a similarly
243 large effect on the voltage at which the PIC reached its maximum in young animals
244 (WT: −43.83±4.79mV, N=19 vs. SOD1: −52.32±4.20mV, N=15; g=−1.83
245 95%CI[−2.63−−1.04]; t(32)=5.50, p=4.8e−06). Similarly to the situation with PIC
246 amplitude, the effect of the SOD1 mutation on its activation voltage was reduced in
247 older animals, at both presymptomatic and symptomatic ages (Table 1).

248 These profound changes in PIC amplitude and activation voltage would be
249 expected to have an impact on the firing properties of motoneurons. We therefore
250 performed current-clamp recordings in the same motoneurons as above. We
251 injected a triangular ramp of current to elicit the repetitive firing of the motoneuron
252 (Figure 2A–B), and measured the voltage threshold for spiking on the first spike
253 triggered by the ramp. In concordance with the hyperpolarization of the PICs,
254 spiking threshold was also hyperpolarized in young animals (WT: −45.35±5.48mV,

N=19 vs. mSOD1: −54.86±5.15mV, N=14; g=−1.74 95%CI[−2.53−−0.81]; t(31)=5.10, p=1.9e−05).

Young adult motoneurons are nonetheless not hyperexcitable

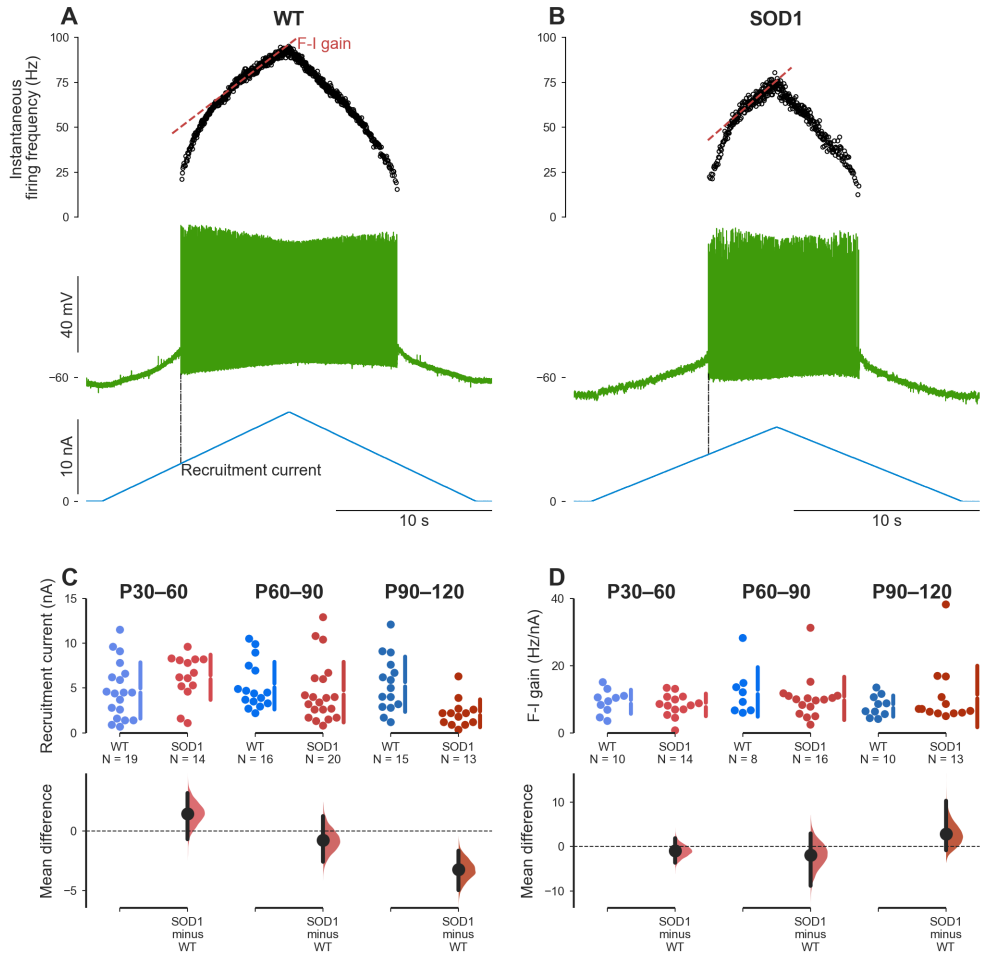

Figure 2. Mutant motoneurons are not hyperexcitable
A. Example of the response of a P101 WT mouse to a triangular ramp of current. From bottom to top, traces are: injected current, membrane potential and instantaneous firing frequency. The dash-dotted line shows the measure of the recruitment current, the current intensity at which the motoneuron starts to fire. The red dashed line shows the linear fit of the firing frequency in the primary range, used to estimate the gain of the F-I relationship. B. Example of the response of a P60 mSOD1 mouse. Same organization as in A. C. Current intensity required for eliciting

the first spike on a triangular ramp of current in WT and mSOD1 motoneurons in each of the age groups. In young adult and presymptomatic mice, mutant motoneurons require the same amount of current than WT motoneuron to fire, P30–60 WT: 4.73±3.14nA, N=19 vs. mSOD1: 6.21±2.51nA, N=14; g=0.50 95%CI[−0.24–1.24]; $t(31)$=−1.51, p=0.14. P60–90 WT: 5.28±2.64nA, N=16 vs. mSOD1: 4.53±3.38nA, N=20; g=−0.24 95%CI[−0.93–0.41]; $t(34)$=0.75, p=0.46. At the symptomatic stages (P90–120), mutant motoneurons exhibit a lower current threshold for firing (WT: 5.43±3.07nA, N=15 vs. mSOD1: 2.19±1.56nA, N=13; g=−1.26 95%CI[−1.95–−0.47]; $t(26)$=3.59, p=0.0017), compatible with the loss of the least excitable cells. D. The slope of the F-I relationship, measured over the primary range, is not affected by the mutation. P30–60 WT: 9.3±3.6Hz/nA, N=10 vs. mSOD1: 8.3±3.4Hz/nA, N=14; g=−0.28 95%CI[−1.10–0.64]; $t(22)$=0.69, p=0.5. P60–90 WT: 12.2±7.3Hz/nA, N=8 vs. mSOD1: 10.3±6.4Hz/nA, N=16; g=−0.27 95%CI[−1.22–0.54]; $t(22)$=0.62, p=0.54. P90–120 WT: 8.0±3.2Hz/nA, N=10 vs. mSOD1: 10.8±9.1Hz/nA, N=13; g=0.38 95%CI[−0.43–0.93]; $t(21)$=−1.04, p=0.31.

Despite the large alterations in PIC amplitude and activation voltage, and despite the change in the voltage threshold for spiking, the excitability of the motoneurons was remarkably unaffected by the SOD1 mutation, regardless of age. Figure 2 shows the response of WT and mSOD1 young adult motoneurons to a slow triangular ramps of current (F-I relationship). We measured the intensity of the current required to elicit the first spike on the ascending ramp ("recruitment current"). Young adult (P30–60) mutant motoneurons, whose neuromuscular junctions are just starting to be denervated, and pre-symptomatic motoneurons (P60–90), which experience substantial denervation, did not require, on average, less current to reach firing threshold than WT controls (Figure 2C). At symptomatic stages (P90–120), the SOD1 mutation does lead to a decrease in the recruitment current compared to WT animals (Figure 2C), which is probably caused by the degeneration of the high threshold motoneurons at this stage.

295 As shown previously (Manuel et al., 2009), most F-I curves, regardless of age and
296 genotype, showed a distinct sub-primary range (SPR) with a steep slope followed by
297 a linear phase called primary range (PR). We used the "gain" of the motoneuron, i.e.
298 the slope of the F-I curve in the PR, as another measure of excitability of
299 motoneurons. Despite the alterations in PICs in mutant motoneurons, the gain of the
300 motoneuron F-I curves were unaffected by both age and mutation (Figure 2D).

301 **Compensatory changes responsible to maintain excitability**

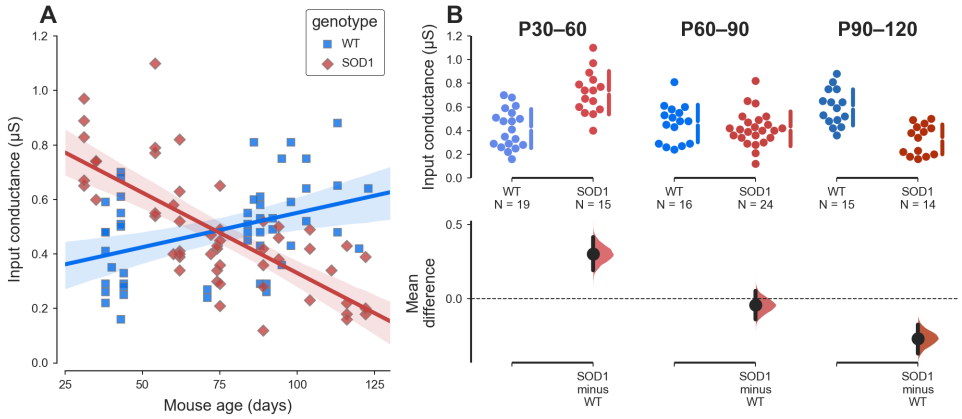

302
303 **Figure 3: Young mutant motoneurons have an aberrantly large input**
304 **conductance**
305 A. Plot of the motoneuron input conductance vs. age in WT (blue squares) and
306 mSOD1 (red diamonds) animals. The solid lines correspond to the linear regression
307 lines with 95% confidence intervals (shaded areas). Pearson correlation coefficients
308 & 95%CI, WT: r=0.40 95%CI[0.14–0.61], p=0.0035, mSOD1: r=−0.73 95%CI[−0.83–
309 −0.57], p=6.1e−10. B. Breakdown of the difference in input conductance between
310 WT and mSOD1 animals by age groups. P30–60 WT: 0.42±0.16µS, N=19 vs. mSOD1:
311 0.72±0.18µS, N=15; g=1.73 95%CI[0.92–2.41]; t(32)=−5.06, p=2.2e−05. P60–90 WT:
312 0.46±0.16µS, N=16 vs. mSOD1: 0.42±0.15µS, N=24; g=−0.28 95%CI[−0.96–0.37];
313 t(38)=0.88, p=0.39. P90–120 WT: 0.60±0.15µS, N=15 vs. mSOD1: 0.33±0.13µS,
314 N=14; g=−1.85 95%CI[−2.57–−1.16]; t(27)=5.16, p=2.1e−05.

315 The fact that young adult motoneurons are not hyperexcitable despite substantial
316 alteration in the PICs suggests that other compensatory mechanisms are acting to
317 preserve the functional output of the cells. Motoneuron input conductance is an

318 important factor controlling neuron excitability. We estimated the input
319 conductance of mSOD1 and WT motoneurons from the slopes of their I-V relations
320 around the level of the resting membrane potential (see Figure 1 and Methods).
321 Input conductances of mSOD1 and WT motoneurons were plotted against the age of
322 the animal in Figure 3A. Consistent with the continuous increase in size of the
323 animals over the age span studied, WT motoneurons exhibit a moderate increase in
324 input conductance in WT motoneurons over time (slope=0.02 μS/week). On the
325 other hand, mSOD1 motoneurons showed the opposite trend (slope=−0.04
326 μS/week). Young adult mutant motoneurons had an input conductance almost twice
327 as high as WT controls at P30–P60 (Figure 3B). This increase is relatively greater (
328 ～1.7 fold) than that observed in neonatal motoneurons at P0–7 (～1.25 fold)
329 (Quinlan et al., 2011), suggesting that the trend for increased conductance has
330 become stronger as the animal matures into the young adult state. However, by the
331 late pre-symptomatic stage (P60–90), the mutation had no longer any effect on
332 input conductance. Finally, symptomatic (P90–120) mSOD1 motoneurons had a
333 smaller input conductance than WT controls, but this difference could be due to the
334 degeneration of the largest, high-threshold units at this stage.

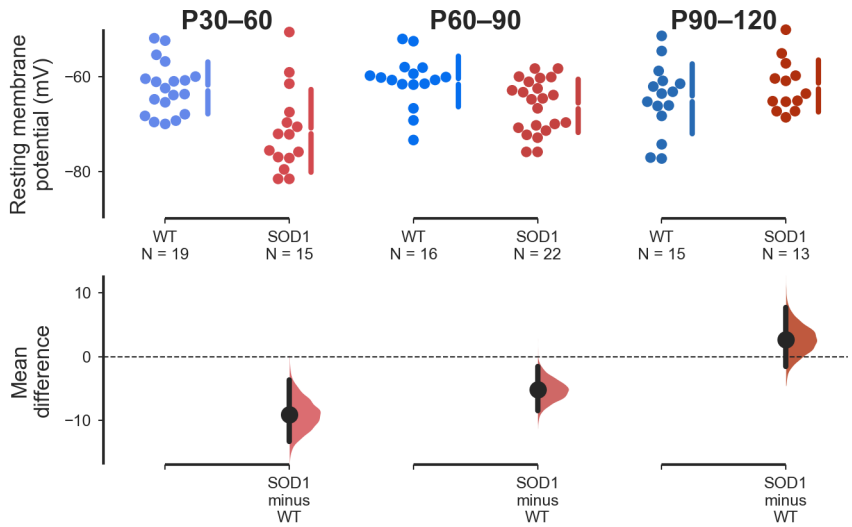

Figure 4. The resting membrane potential of young adult mutant mice is hyperpolarized

Breakdown of the difference in input conductance between WT and mSOD1 animals by age groups. P30–60 WT: −62.38±5.52mV, N=19 vs. mSOD1: −71.45±8.78mV, N=15; g=−1.24 95%CI[−2.13–−0.23]; $t(32)$=3.49, p=0.002. P60–90 WT: −60.98±5.35mV, N=16 vs. mSOD1: −66.18±5.63mV, N=22; g=−0.92 95%CI[−1.54–−0.18]; $t(36)$=2.89, p=0.0067. P90–120 WT: −64.71±7.42mV, N=15 vs. mSOD1: −61.99±5.43mV, N=13; g=0.40 95%CI[−0.35–1.10]; $t(26)$=−1.12, p=0.27.

The increase in input conductance is not the only compensatory change happening in young adult mutant motoneurons. In particular, one would have expected the leftward shift in the activation voltage of PICs seen in these motoneurons to have a profound impact on their firing behavior. This discrepancy can be explained by a parallel almost 10 mV hyperpolarization of the resting membrane potential in young adult mSOD1 motoneurons (Figure 4, P30–60). This effect is still observable at pre-symptomatic stages, but to a lesser degree (Figure 4, P60–90). At symptomatic ages, however, mutant motoneurons had similar resting membrane potentials as WT controls (Figure 4, P90–120).

353 When taking into account this hyperpolarization of the resting membrane
354 potential, the relative values of the voltage threshold for spiking (ΔV_{th}, difference
355 between the voltage threshold and the resting membrane potential), as well as the
356 relative activation voltage of the PICs (ΔV_{PIC}) and the relative voltage at the peak of
357 the PIC (ΔV_{peak}) were all similar between WT and mSOD1 motoneuron regardless of
358 age (Table 1), which suggest that these are the quantities that are homeostatically
359 regulated.

360 ## Arms race between PICs and input conductance

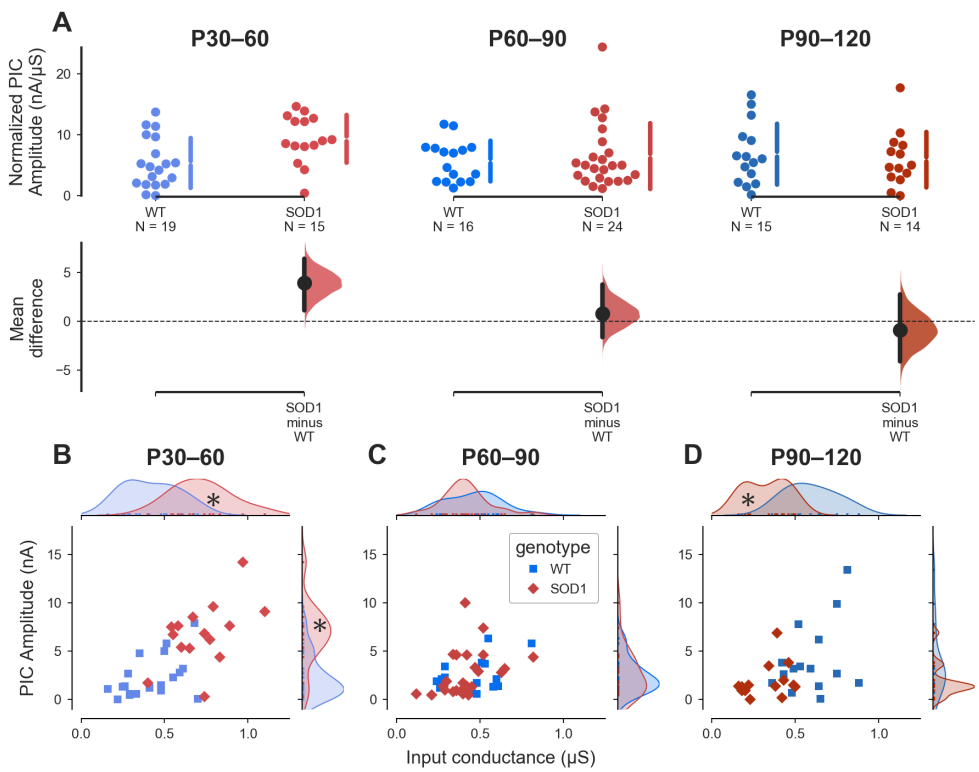

361
362 **Figure 5. Some motoneurons exhibit properties outside of the normal range**
363 A. Breakdown of the difference in normalized PIC amplitude (PIC amplitude divided
364 by input conductance) between WT and mSOD1 animals by age groups. P30–60 WT:
365 5.35±4.11nA/μS, N=19 vs. mSOD1: 9.32±3.94nA/μS, N=15; g=0.96 95%CI[0.16–
366 1.76]; $t(32)$=−2.86, p=0.0075. P60–90 WT: 5.65±3.35nA/μS, N=16 vs. mSOD1:
367 6.46±5.39nA/μS, N=24; g=0.17 95%CI[−0.50–0.66]; $t(38)$=−0.59, p=0.56. P90–120

WT: 6.80±5.01nA/μS, N=15 vs. mSOD1: 5.93±4.53nA/μS, N=14; g=−0.18 95%CI[−0.88–0.63]; $t(27)$=0.49, p=0.63. B. Plot of the PIC amplitude vs. the input conductance of young adult motoneurons (P30–60) in WT (blue squares) and mSOD1 (red diamonds) animals. The marginal plots indicate the kernel density estimation of the distributions of the values in the two populations. The asterisks indicate point to fraction of the mSOD1 population that is outside the range of the WT population. C. Same as A for the presymptomatic age range P60–90. D. Same as A for the symptomatic age range P90–120.

Our results show that, during the disease progression, motoneurons are actively engaged in a homeostatic process to maintain their firing output. It is plausible that this process would, by itself, cause undue stress to the cell. For example, the ratio of PIC to conductance is a major determinant of net excitability (Huh et al., 2017). If these two parameters grow in proportion, then net excitability is likely to stay about the same. We thus analyzed PIC amplitudes normalized by input conductances (Figure 5A). Although pre-symptomatic and symptomatic cells manage to maintain a normal normalized-PIC amplitudes, young adult mSOD1 motoneurons have a larger normalized PIC amplitude than their WT controls (Figure 5A). This implies that, in these animals, the cells that are abnormally large (large input conductance) also have PICs that are larger than expected for their size. It is likely that these cells are under considerable stress to respond to the high metabolic demand imposed by their large size, as well as the potential massive influx of calcium caused by their abnormally large PICs.

This effect is also visible in the plots of Figure 5B–D showing the relationship between PIC amplitude and input conductance. In the young adult animals (Figure 5B), the majority of the mutant motoneurons are clustered in the upper right hand corner, with values of both conductances and PIC amplitudes that are outside of the

range of WT controls. At the pre-symptomatic stages, the WT and mSOD1 populations roughly overlap (Figure 5C), and at the symptomatic ages, the situation is reversed, with the appearance of a cluster (N=6) of very small cells (asterisk in Figure 5D), most of which also have very small PICs. These results show that the overall initial increase in PIC and conductance amplitudes driven by the SOD1 mutation generates a sub-population of motoneurons with conductance and PIC amplitudes that are actually above those of the normal, WT range (P30–60). The steady reduction in these amplitudes is so strong that by P90–120, a sub-population develops that falls below the normal range.

Hypoexcitable cells

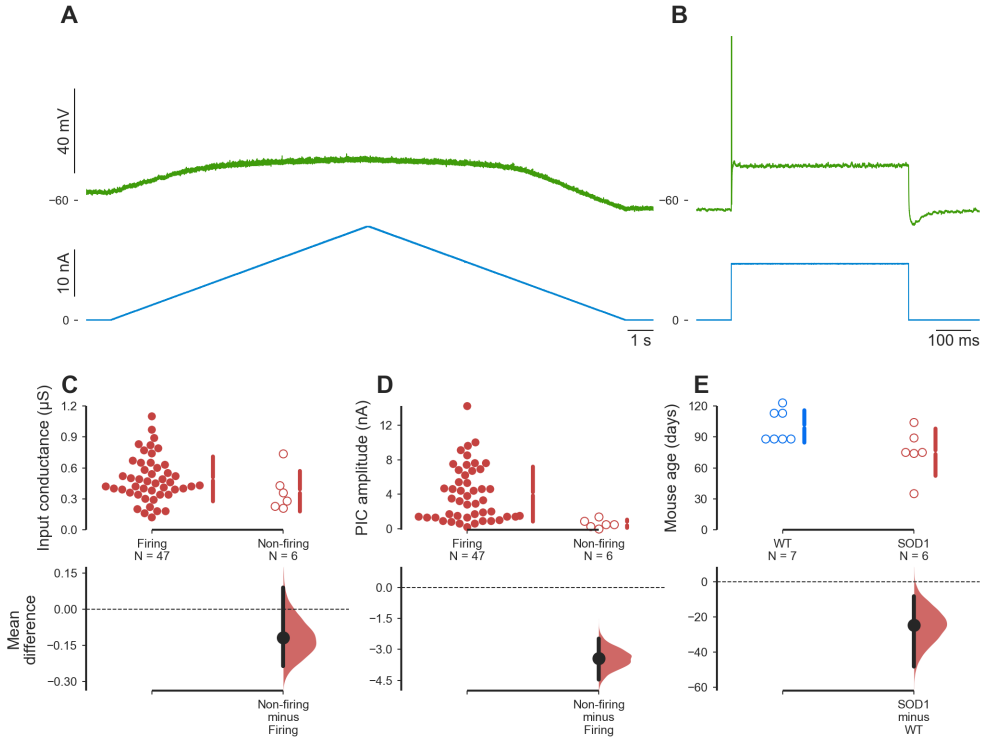

Figure 6: Some cells are hypoexcitable and cannot fire repetitively

A. Example of a mSOD1 motoneuron (from a P88 mouse) that is unable to fire repetitively in response to a triangular ramp of current. Top trace: membrane potential, bottom trace: injected current. B. This same motoneuron was able to generate a single full-height action potential in response to a square pulse of current. Same organization as in A. C. Non-firing motoneurons had a similar input conductance compared to motoneurons that were able to fire repetitively. Firing: 0.49±0.22µS, N=47 vs. non-firing: 0.38±0.20µS, N=6; g=−0.54 95%CI[−1.11–0.50]; t(51)=1.36, p=0.22 D. Non-firing motoneurons had much smaller PICs than motoneurons able to fire repetitively. Firing: Firing: 4.04±3.18nA, N=47 vs. non-firing: 0.60±0.49nA, N=6; g=−1.12 95%CI[−1.42−−0.86]; t(51)=6.81, p=1.3e−08 E. Non-firing motoneurons appear earlier in mSOD1 animals compared to WT animals. WT: 100±16 days old, N=7 vs. SOD1: 75±23 days old, N=6; g=−1.20 95%CI[−2.06–0.01]; t(11)=2.24, p=0.053

As previously shown (Delestrée et al., 2014; Martínez-Silva et al., 2018), mSOD1 motoneuron tend to lose their ability to fire repetitively as the disease progresses. In the present study, out of the 53 mutant motoneurons recorded, 6 motoneurons could not fire repetitively to current ramps despite still being able to fire a single or a few action potentials to current steps. Figure 8 shows an example of such a motoneuron. Although those cells were not, on average, larger than those that fired repetitively (Figure 6B), non-firing cells were characterized by a very PIC amplitude (Figure 6C, see also (Huh et al., 2017)). Even more striking were the difference in PIC amplitude normalized by the input conductance of the cells. Non-firing motoneurons had a much smaller normalized PIC amplitude (1.91±1.82nA/µS, N=6) compared to repetitively firing motoneurons (7.80±4.79nA/µS, N=47; g=−1.27 95%CI[−1.65−−0.80]; t(51)=5.77, p=2.6e−05). Finally, although some non-firing motoneurons could be found in WT mice, non-firing motoneurons appear on average 25 days earlier in mSOD1 mice (Figure 6D).

Table 1: summary of the properties of the motoneurons, broken down by age range

The table shows the various properties that were measured in each motoneuron. The rows are sorted in descending order of effect size at P30–60. WT and mSOD1 columns show mean values ± standard deviation, with the 95%CI around the mean below. The "Mean diff." column shows the mean difference between mSOD1 and WT population, with 95% CI below. The "Hedges' *g*" column shows a graphical representation of the effect size. ΔF: difference between the instantaneous firing frequency at de-recruitment and at recruitment. ΔI: difference between the de-recruitment and recruitment currents. ΔV_{th}: voltage threshold for spiking relative to the resting membrane potential. ΔV_{PIC}: PIC onset voltage relative to the resting membrane potential. ΔV_{peak}: voltage at the peak of the PICs relative to the resting membrane potential

Discussion

In this paper, we studied how motoneuron electrical properties evolve over the time course of ALS, focusing particularly on the persistent inward currents (PICs). We show that, in young adult mutant mice, before and up to the time where denervations are just starting, PICs are abnormally large compared to controls. This increase in PIC amplitude is accompanied by a parallel increase in motoneuron input conductance with the net effect that the excitability of the cells remains normal. Later, while the animals remain pre-symptomatic but denervation has begun, motoneuron properties return to normal levels. Finally, in symptomatic animals, mutant motoneurons tend to have smaller input conductance and smaller recruitment current.

Homeostatic regulation of motoneuron output

Although ALS is classically considered an adult-onset disease, we know from earlier studies of motoneurons in animal models of ALS that the change in motoneurons' intrinsic excitability is the first sign to be seen in the pathogenesis, long before any overt motor deficits manifest. Hyperexcitability is observed in

462 cultured E13 spinal motoneurons (Kuo et al., 2004), E15 cortical motoneurons (Pieri
463 et al., 2009), E17.5 spinal motoneurons (Martin et al., 2013 p.20), as well as early
464 postnatal hypoglossal motoneurons (van Zundert et al., 2008). Consequently, the
465 motor system in general, and motoneurons in particular, must exhibit remarkable
466 capability for homeostatic regulation to maintain a quasi-normal motor output until
467 overt symptoms appear, but there are many combinations of intrinsic properties
468 that can produce the same firing pattern (Marder and Goaillard, 2006). In neonatal
469 mSOD1 mice, the majority of motoneurons exhibited normal excitability (based on
470 recruitment current and F-I gain), although the most resistant population of
471 motoneuron seem to retain some hyperexcitability (Quinlan et al., 2011; Leroy et al.,
472 2014). Yet, PICs were almost twice as large in mutant compared to WT neonatal
473 motoneurons. This increased PIC amplitude was seemingly compensated by a
474 parallel increase in input conductance (Quinlan et al., 2011). In young adult animals,
475 this trend seems to continue, as the present study demonstrated an almost 3×
476 increase in PIC amplitude, accompanied by an almost 2× increase in input
477 conductance. Similarly, we observed large changes in PIC onset and peak voltages,
478 compensated by a commensurate hyperpolarization of the resting membrane
479 potential. These trends with disease progression from the neonatal state through
480 development of severe symptoms are summarized in Figure 7. An overall pattern of
481 oscillations is evident, with the PIC oscillations tending to increase excitability but
482 the conductance and rest potential oscillations tending to reduce it.

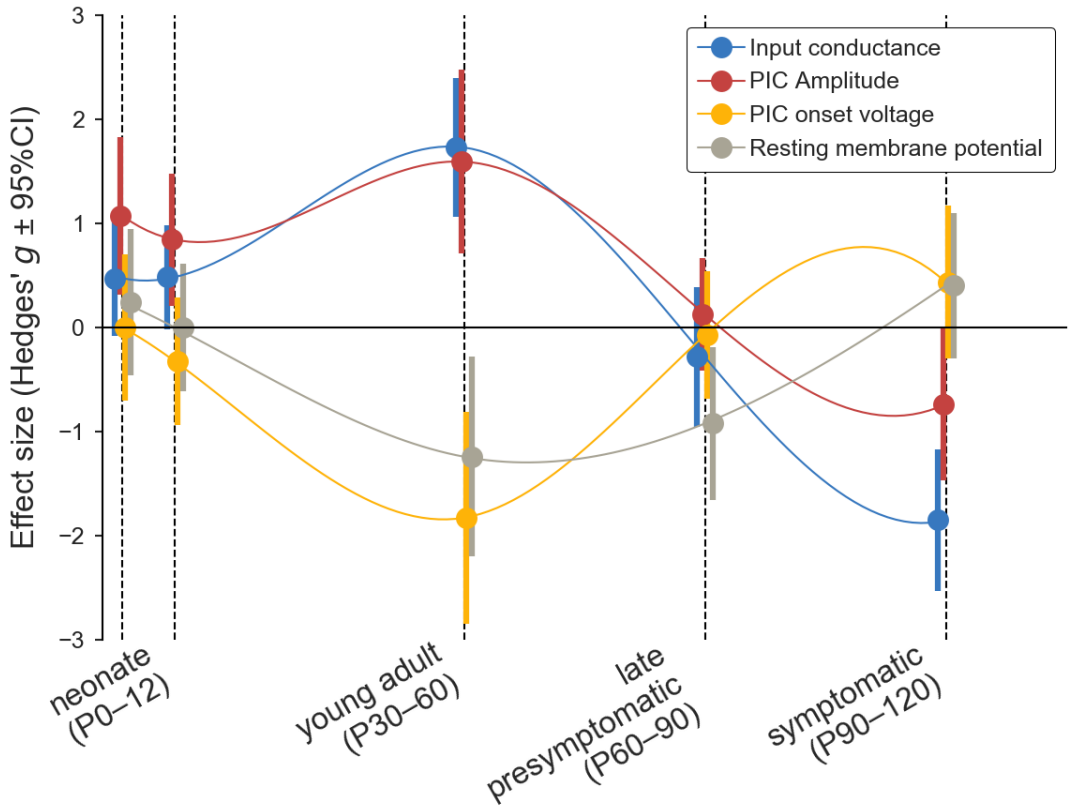

Figure 7: summary of the changes in motoneuron properties over time
Schematic representation of the changes in four key electrophysiological properties over time. The dots represent the effect size (Hedges' g) and the vertical bars show the 95%CI around g. The thin lines are cubic splines interpolation of the data over time. The points have been slightly staggered so that the vertical bars do not occlude each other. Data from neonates (P0–5 and P6–12) are from Quinlan et al. (2011).

The properties of the motoneurons seem to normalize at the late pre-symptomatic stage (P60–90), but it is unclear whether this is due to changes in the homeostatic pathways involved, or whether it is caused by the start of the degeneration process in the most vulnerable motoneurons. At symptomatic stages, motoneurons appear to be hypoexcitable. They have a smaller input conductance (Figure 3), and smaller recruitment current (Figure 2), but that most likely reflect the fact that the largest cells have degenerated by this age, and that the remaining cells may have shrunk (see below, and Dukkipati et al., 2018).

498 ## The hidden cost of homeostatic regulation

499 Although the degeneration of motoneurons in ALS constitutes a failure in cell
500 homeostasis, our results show that, throughout the "silent", presymptomatic phase
501 of ALS, motoneurons are actively engaged in a highly successful homeostatic process
502 to maintain their firing output. However, this process is not perfect, and, by itself,
503 could be a major source of stress for the cells. We do not know whether the cells
504 increase their conductance to compensate for the fast increase in PICs or *vice versa*,
505 but the end result is the appearance of cells with both input conductance and PIC
506 amplitudes outside of the normal range (Figure 5B). The increase in input
507 conductance could be due to the insertion of more channels in the membrane.
508 However, direct measurements of soma sizes have revealed that pre-symptomatic
509 mutant cells are physically larger than controls (Shoenfeld et al., 2014; Dukkipati et
510 al., 2018). This increase in size, coupled with the larger calcium entry in the cells due
511 to the larger PICs (which are in part calcium-medicated (Li and Bennett, 2003)), is
512 bound to cause undue metabolic stress on those cells that are outside of the normal
513 range, despite the fact that cells manage to maintain a normal output. These cells are
514 likely to be Fast Fatigable (FF) motoneurons, as they are the cells with the largest
515 input conductance, and the largest PICs (Lee and Heckman, 1998; Huh et al., 2017)
516 in normal conditions, and they are the cells that are the most vulnerable to ALS (Pun
517 et al., 2006; Hegedus et al., 2007, 2008).

518 As the disease progresses, those large, vulnerable cells become the first
519 motoneurons that will embark on a degeneration pathway (Saxena et al., 2009,
520 2013; Martínez-Silva et al., 2018), and will lose their ability to fire repetitively

521 (Martínez-Silva et al., 2018). This early loss of the large cells is consistent with stress
522 induced by aberrantly large conductances and PICs. This loss is also likely the
523 primary reason why motoneurons appear to recover normal properties at late pre-
524 symptomatic stages. Nevertheless, it is probable that all motoneurons, regardless of
525 type, experience this form of stress. Interestingly, we observed that some of the
526 smallest motoneurons, which are the most resistant to the disease, appear to shrink
527 in the oldest animals (Figure 5D), consistent with anatomical observations (Kiernan
528 and Hudson, 1991; Dukkipati et al., 2018). At this point, it is unclear whether this
529 shrinkage is a pathological feature or a strong homeostatic effort by the surviving
530 motoneurons to counteract the stress generated by their initial hypertrophy.

531 **Hyper-vigilant homeostasis**

532 Mitchell and colleagues have recently proposed that cellular homeostasis is in
533 ALS motoneurons is in fact too strong (Mitchell and Lee, 2012; Irvin et al., 2015).
534 Several aspects of our results are consistent with this hyper-vigilant homeostasis
535 hypothesis. A major impetus for this hypothesis was that meta-analyses of data
536 obtained from many studies on multiple cellular properties revealed patterns of
537 oscillations as the disease progressed, suggesting the existence of high feedback
538 gains for homeostatic processes. Similar oscillations are clearly present in our
539 results, as illustrated in Figure 7. The highly successful homeostasis for net
540 excitability, achieved at the cost of excessively high amplitudes for conductances
541 and PICs, clearly shows homeostasis is strong. The development of subpopulations
542 that are initially well above and then well below the normal range supports the
543 possibility that this strong homeostasis is excessive. Direct tests of the hyper-

544 vigilant homeostasis hypothesis will require quantitative comparisons of the
545 responses of ALS and WT motoneurons to controlled homeostatic challenges.

546 ### Comparison with previous studies

547 The present study displays some differences with other studies, including by our
548 own. Others have described signs of hyperexcitability in spinal motoneurons
549 (Meehan et al., 2010; Jensen et al., 2020), and in the motor cortex (Kim et al., 2017),
550 accompanied with changes in local circuitry (Hedegaard et al., 2015; Kim et al.,
551 2017; Bączyk et al., 2020; Jara et al., 2020), although that aspect was not
552 investigated in the present work. We have previously studied the properties of
553 motoneurons in the same SOD1(G93A) mouse model of ALS group (Delestrée et al.,
554 2014; Martínez-Silva et al., 2018) but have mainly focused on a short period of time
555 just at the onset of denervations (P45–55). Although that time point partly overlaps
556 with the present young adult stage, we had not detected differences in input
557 conductances (Martínez-Silva et al., 2018). This might be due to the fact that the
558 difference in input conductance is largest at earlier time points (Figure 3A). Indeed,
559 the difference is gone at P60–90, and we did report an increase in input conductance
560 in an earlier series of experiments, which was more pronounced at younger time
561 points (Delestrée et al., 2014). Similarly, we did not detect a difference in resting
562 membrane potential in the Martínez-Silva et al. (2018) study. Again, the discrepancy
563 could be due to the difference in the distributions of the ages of the animals studied.
564 It is also possible that, despite our best efforts, the disease is not following the exact
565 same time course in the two colonies used (the present paper is based on animals
566 bred at Northwestern University in Chicago, while our previous studies were

567 conducted on animals bred in Paris). It is therefore conceivable that even though the
568 ages overlap, those ages correspond to slightly different stages of the disease.

569 In the present study, we recorded only 13 motoneurons out of 103 (7/50 WT and
570 6/53 mSOD1) that were unable to fire repetitively, contrary to our previous study
571 where we showed that a large proportion of vulnerable motoneurons became
572 hypoexcitable before the onset of denervation (P45–55, Martínez-Silva et al., 2018).
573 This discrepancy could be explained by the experimental constraints of the present
574 study. Indeed, obtaining stable voltage clamp recordings in vivo in mice is quite a
575 challenge, requiring electrodes able to pass very large amounts of current and
576 motoneuron able to withstand the protocol. Since we have only included for analysis
577 cells in which the voltage clamp protocol was completed successfully, we
578 hypothesize that we may have biased our sample towards the healthiest cells that
579 have yet to take the path of degeneration.

580 **Limitations**

581 The results presented here have been collected on the SOD1(G93A) mouse model
582 of ALS, a model that has attracted criticisms due to it being an overexpression
583 model, and its failure to bring seemingly promising therapies to the clinic (Philips
584 and Rothstein, 2015). Nevertheless, some parallel with other studies suggest that
585 our results could be extended to other models. First, Meehan et al. (2010) have
586 studied an unrelated mSOD1(G127X) model and have shown that although the net
587 excitability of the motoneurons was not affected by the mutation, there were
588 nonetheless signs of increased PICs in these motoneurons. Second, we observed

589 that, in late symptomatic animals, some cells exhibited a very small input
590 conductance, well below the normal range at this age, suggesting that these cells
591 actually shrank. This observation matches morphological measurements in mSOD1
592 mice (Dukkipati et al., 2018), but also observations from sporadic human patients
593 (Kiernan and Hudson, 1991).

594 We demonstrated a remarkably successful homeostatic control of motoneuron
595 firing, that we can attribute to commensurate changes in PICs and input
596 conductance. However, it is likely that other currents are also implicated in this
597 process (Marder and Goaillard, 2006). Limitations inherent to in vivo
598 electrophysiology prevent us from isolating many different currents and further in
599 vitro investigations in adults (Jiang and Heckman, 2006; Mitra and Brownstone,
600 2011; Jiang et al., 2017; Bhumbra and Beato, 2018) are warranted to shed more light
601 on the panoply of channels involved in this process.

602 Conclusion

603 Overall, our results show homeostasis for net excitability in mutant SOD1
604 motoneurons is remarkably strong in the presymptomatic state. This success
605 however comes at a cost of large compensatory changes in basic electrical
606 properties. These results support the hypothesis that ALS is not due to a single
607 specific root cause but instead caused by an inherent instability at the system-level
608 (Mitchell and Lee, 2012), possibly caused by an "hyper-vigilant" homeostatic system
609 in motoneurons. Initial perturbations in the electrical properties of motoneurons
610 would be overcompensated for, leading to new sources of stress, which, in turn,

611 would be overcorrected, and so on and so forth until the metabolic burden becomes
612 too high to sustain for the motoneuron. FF motoneurons have higher metabolic
613 needs (Le Masson et al., 2014) and lower calcium-buffering capabilities
614 (Grosskreutz et al., 2010) in the first place, which make them particularly vulnerable
615 to this vicious cycle.

616 Data availability

617 Data files and a computational notebook allowing reproducing the analysis and
618 figures of this article are provided at the URL:
619 http://doi.org/10.5281/zenodo.3831947

620 References

621 Bączyk M, Alami NO, Delestrée N, Martinot C, Tang L, Commisso B, Bayer D, Doisne
622 N, Frankel W, Manuel M, Roselli F, Zytnicki D (2020) Synaptic restoration by
623 cAMP/PKA drives activity-dependent neuroprotection to motoneurons in ALS. J Exp
624 Med 217 Available at: https://rupress-
625 org.insb.bib.cnrs.fr/jem/article/217/8/e20191734/151829/Synaptic-restoration-
626 by-cAMP-PKA-drives-activity [Accessed June 2, 2020].

627 Bernard C (2019) Changing the Way We Report, Interpret, and Discuss Our Results
628 to Rebuild Trust in Our Research. eNeuro 6 Available at:
629 https://www.eneuro.org/content/6/4/ENEURO.0259-19.2019 [Accessed April 13,
630 2020].

631 Bhumbra GS, Beato M (2018) Recurrent excitation between motoneurones
632 propagates across segments and is purely glutamatergic. PLOS Biol 16:e2003586
633 Available at:
634 https://journals.plos.org/plosbiology/article?id=10.1371/journal.pbio.2003586
635 [Accessed May 7, 2020].

636 Brownstone RM, Lancelin C (2018) Escape from homeostasis: spinal microcircuits
637 and progression of amyotrophic lateral sclerosis. J Neurophysiol 119:1782–1794
638 Available at: https://www.physiology.org/doi/full/10.1152/jn.00331.2017
639 [Accessed October 25, 2018].

640 Cumming G (2012) Understanding the new statistics: effect sizes, confidence

641 intervals, and meta-analysis. New York: Routledge, Taylor & Francis Group.

642 Delestrée N, Manuel M, Iglesias C, Elbasiouny SM, Heckman CJ, Zytnicki D (2014)
643 Adult spinal motoneurones are not hyperexcitable in a mouse model of inherited
644 amyotrophic lateral sclerosis. J Physiol 592:1687–703 Available at:
645 http://www.ncbi.nlm.nih.gov/pubmed/24445319.

646 Dukkipati SS, Garrett TL, Elbasiouny SM (2018) The vulnerability of spinal
647 motoneurons and soma size plasticity in a mouse model of amyotrophic lateral
648 sclerosis. J Physiol 596:1723–1745.

649 Grosskreutz J, van den Bosch L, Keller BU (2010) Calcium dysregulation in
650 amyotrophic lateral sclerosis. Cell Calcium 47:165–174 Available at:
651 https://doi.org/10.1016/j.ceca.2009.12.002.

652 Hedegaard A, Lehnhoff J, Moldovan M, Grøndahl L, Petersen NC, Meehan CF (2015)
653 Postactivation depression of the Ia EPSP in motoneurons is reduced in both the
654 G127X SOD1 model of amyotrophic lateral sclerosis and in aged mice. J
655 Neurophysiol 114:1196–210.

656 Hedges LV (2016) Distribution Theory for Glass's Estimator of Effect size and
657 Related Estimators: J Educ Stat Available at:
658 https://journals.sagepub.com/doi/10.3102/10769986006002107 [Accessed May 7,
659 2020].

660 Hegedus J, Putman CT, Gordon T (2007) Time course of preferential motor unit loss
661 in the SOD1 G93A mouse model of amyotrophic lateral sclerosis. Neurobiol Dis
662 28:154–164 Available at: https://doi.org/10.1016/j.nbd.2007.07.003.

663 Hegedus J, Putman CT, Tyreman N, Gordon T (2008) Preferential motor unit loss in
664 the SOD1 G93A transgenic mouse model of amyotrophic lateral sclerosis. J Physiol
665 586:3337–3351 Available at: https://doi.org/10.1113/jphysiol.2007.149286.

666 Ho J, Tumkaya T, Aryal S, Choi H, Claridge-Chang A (2019) Moving beyond P values:
667 data analysis with estimation graphics. Nat Methods 16:565–566 Available at:
668 https://www-nature-com.insb.bib.cnrs.fr/articles/s41592-019-0470-3 [Accessed
669 December 30, 2019].

670 Huh S, Siripuram R, Lee RH, Turkin VV, O'Neill D, Hamm TM, Heckman CJ, Manuel M
671 (2017) PICs in motoneurons do not scale with the size of the animal: a possible
672 mechanism for faster speed of muscle contraction in smaller species. J Neurophysiol
673 118:93–102 Available at: https://doi.org/10.1152/jn.00045.2017.

674 Hunter JD (2007) Matplotlib: A 2D Graphics Environment. Comput Sci Eng 9:90–95.

675 Ilieva H, Polymenidou M, Cleveland DW (2009) Non-cell autonomous toxicity in
676 neurodegenerative disorders: ALS and beyond. J Cell Biol 187:761–772 Available at:
677 https://doi.org/10.1083/jcb.200908164.

678 Irvin CW, Kim RB, Mitchell CS (2015) Seeking homeostasis: temporal trends in
679 respiration, oxidation, and calcium in SOD1 G93A Amyotrophic Lateral Sclerosis
680 mice. Front Cell Neurosci 9:248.

681 Jara JH, Sheets PL, Nigro MJ, Perić M, Brooks C, Heller DB, Martina M, Andjus PR,
682 Ozdinler PH (2020) The Electrophysiological Determinants of Corticospinal Motor
683 Neuron Vulnerability in ALS. Front Mol Neurosci 13:73.

684 Jensen DB, Kadlecova M, Allodi I, Meehan CF (2020) Spinal motoneurones are
685 intrinsically more responsive in the adult G93A SOD1 mouse model of Amyotrophic
686 Lateral Sclerosis. J Physiol n/a Available at:
687 https://physoc.onlinelibrary.wiley.com/doi/abs/10.1113/JP280097 [Accessed July
688 28, 2020].

689 Jiang MC, Adimula A, Birch D, Heckman CJ (2017) Hyperexcitability in synaptic and
690 firing activities of spinal motoneurons in an adult mouse model of amyotrophic
691 lateral sclerosis. Neuroscience 362:33–46.

692 Jiang MC, Heckman CJ (2006) In vitro sacral cord preparation and motoneuron
693 recording from adult mice. J Neurosci Off J Soc Neurosci 156:31–36 Available at:
694 https://doi.org/10.1016/j.jneumeth.2006.02.002.

695 Johnson MD, Heckman CJ (2010) Interactions between focused synaptic inputs and
696 diffuse neuromodulation in the spinal cord. Ann N Y Acad Sci 1198:35–41 Available
697 at: https://doi.org/10.1111/j.1749-6632.2010.05430.x.

698 Kanning KC, Kaplan A, Henderson CE (2009) Motor neuron diversity in development
699 and disease. Annu Rev Neurosci 33:409–440 Available at:
700 https://doi.org/10.1146/annurev.neuro.051508.135722.

701 Kiernan JA, Hudson AJ (1991) Changes in Sizes of Cortical and Lower Motor Neurons
702 in Amyotrophic Lateral Sclerosis. Brain 114:843–853 Available at:
703 https://academic-oup-com.insb.bib.cnrs.fr/brain/article/114/2/843/263744
704 [Accessed April 13, 2020].

705 Kim J, Hughes EG, Shetty AS, Arlotta P, Goff LA, Bergles DE, Brown SP (2017)
706 Changes in the Excitability of Neocortical Neurons in a Mouse Model of Amyotrophic
707 Lateral Sclerosis Are Not Specific to Corticospinal Neurons and Are Modulated by
708 Advancing Disease. J Neurosci Off J Soc Neurosci 37:9037–9053.

709 Kuo JJ, Schonewille M, Siddique T, Schults ANA, Fu R, Bär PR, Anelli R, Heckman CJ,
710 Kroese ABA (2004) Hyperexcitability of cultured spinal motoneurons from
711 presymptomatic ALS mice. J Neurophysiol 91:571–575 Available at:
712 https://doi.org/10.1152/jn.00665.2003.

713 Le Masson G, Przedborski S, Abbott LF (2014) A Computational Model of Motor
714 Neuron Degeneration. Neuron 83:758–760 Available at:
715 http://www.ncbi.nlm.nih.gov/pubmed/25088365.

716 Lee RH, Heckman CJ (1998) Bistability in spinal motoneurons in vivo: systematic
717 variations in persistent inward currents. J Neurophysiol 80:583–593.

718 Leroy F, Lamotte d'Incamps B, Imhoff-Manuel RD, Zytnicki D (2014) Early intrinsic
719 hyperexcitability does not contribute to motoneuron degeneration in amyotrophic
720 lateral sclerosis. eLife 3 Available at:
721 http://www.ncbi.nlm.nih.gov/pubmed/25313866.

722 Li Y, Bennett DJ (2003) Persistent sodium and calcium currents cause plateau
723 potentials in motoneurons of chronic spinal rats. J Neurophysiol 90:857–869
724 Available at: https://doi.org/10.1152/jn.00236.2003.

725 Makin TR, Orban de Xivry J-J (2019) Ten common statistical mistakes to watch out
726 for when writing or reviewing a manuscript Rodgers P, Parsons N, Holmes N, eds.
727 eLife 8:e48175 Available at: https://doi.org/10.7554/eLife.48175 [Accessed
728 October 28, 2019].

729 Manuel M, Heckman CJ (2011) Adult mouse motor units develop almost all of their
730 force in the subprimary range: a new all-or-none strategy for force recruitment? J
731 Neurosci 31:15188–15194 Available at:
732 http://www.ncbi.nlm.nih.gov/pubmed/22016552.

733 Manuel M, Iglesias C, Donnet M, Leroy F, Heckman CJ, Zytnicki D (2009) Fast
734 kinetics, high-frequency oscillations, and subprimary firing range in adult mouse
735 spinal motoneurons. J Neurosci 29:11246–11256 Available at:
736 http://www.ncbi.nlm.nih.gov/pubmed/19741131.

737 Marder E, Goaillard J-M (2006) Variability, compensation and homeostasis in
738 neuron and network function. Nat Rev Neurosci 7:563–574.

739 Martin E, Cazenave W, Cattaert D, Branchereau P (2013) Embryonic alteration of
740 motoneuronal morphology induces hyperexcitability in the mouse model of
741 amyotrophic lateral sclerosis. Neurobiol Dis 54:116–26.

742 Martínez-Silva M de L, Imhoff-Manuel RD, Sharma A, Heckman C, Shneider NA,
743 Roselli F, Zytnicki D, Manuel M (2018) Hypoexcitability precedes denervation in the
744 large fast-contracting motor units in two unrelated mouse models of ALS Rubin LL,
745 ed. eLife 7:e30955 Available at: https://doi.org/10.7554/eLife.30955 [Accessed
746 February 7, 2019].

747 McKinney W (2011) pandas: a foundational Python library for data analysis and
748 statistics. Python High Perform Sci Comput 14.

749 Meehan CF, Moldovan M, Marklund SL, Graffmo KS, Nielsen JB, Hultborn H (2010)
750 Intrinsic properties of lumbar motor neurones in the adult G127insTGGG
751 superoxide dismutase-1 mutant mouse in vivo: evidence for increased persistent
752 inward currents. Acta Physiol Oxf Engl 200:361–76.

753 Michel MC, Murphy TJ, Motulsky HJ (2020) New Author Guidelines for Displaying
754 Data and Reporting Data Analysis and Statistical Methods in Experimental Biology.
755 Mol Pharmacol 97:49–60 Available at:
756 http://molpharm.aspetjournals.org/lookup/doi/10.1124/mol.119.118927
757 [Accessed January 13, 2020].

758 Mitchell CS, Lee RH (2012) Dynamic Meta-Analysis as a Therapeutic Prediction Tool
759 for Amyotrophic Lateral Sclerosis. In: Amyotrophic Lateral Sclerosis (Maurer M, ed).
760 InTech. Available at: http://www.intechopen.com/books/amyotrophic-lateral-
761 sclerosis/dynamic-meta-analysis-as-a-therapeutic-prediction-tool-for-amyotrophic-
762 lateral-sclerosis [Accessed January 5, 2020].

763 Mitra P, Brownstone RM (2011) An in vitro spinal cord slice preparation for
764 recording from lumbar motoneurons of the adult mouse. J Neurophysiol 107:728–
765 741 Available at: https://www.physiology.org/doi/full/10.1152/jn.00558.2011
766 [Accessed December 6, 2018].

767 Philips T, Rothstein JD (2015) Rodent Models of Amyotrophic Lateral Sclerosis. Curr
768 Protoc Pharmacol Editor Board SJ Enna Ed--Chief Al 69:5.67.1-5.67.21 Available at:
769 https://www.ncbi.nlm.nih.gov/pmc/articles/PMC4562058/ [Accessed April 13,
770 2020].

771 Pieri M, Carunchio I, Curcio L, Mercuri NB, Zona C (2009) Increased persistent
772 sodium current determines cortical hyperexcitability in a genetic model of
773 amyotrophic lateral sclerosis. Exp Neurol 215:368–379 Available at:
774 https://doi.org/10.1016/j.expneurol.2008.11.002.

775 Pun S, Santos AF, Saxena S, Xu L, Caroni P (2006) Selective vulnerability and pruning
776 of phasic motoneuron axons in motoneuron disease alleviated by CNTF. Nat
777 Neurosci 9:408–19 Available at: http://www.ncbi.nlm.nih.gov/pubmed/16474388.

778 Quinlan KA, Schuster JE, Fu R, Siddique T, Heckman CJ (2011) Altered postnatal
779 maturation of electrical properties in spinal motoneurons in a mouse model of
780 amyotrophic lateral sclerosis. J Physiol 589:2245–2260 Available at:
781 http://eutils.ncbi.nlm.nih.gov/entrez/eutils/elink.fcgi?dbfrom=pubmed&id=21486
782 770&retmode=ref&cmd=prlinks.

783 Rosen DR, Siddique T, Patterson D, Figlewicz DA, Sapp P, Hentati A, Donaldson D,
784 Goto J, O'Regan JP, Deng H-X (1993) Mutations in Cu/Zn superoxide dismutase gene
785 are associated with familial amyotrophic lateral sclerosis. Nature 362:59–62
786 Available at: https://doi.org/10.1038/362059a0.

787 Saxena S, Cabuy E, Caroni P (2009) A role for motoneuron subtype-selective ER
788 stress in disease manifestations of FALS mice. Nat Neurosci 12:627–636 Available
789 at: https://doi.org/10.1038/nn.2297.

790 Saxena S, Roselli F, Singh K, Leptien K, Julien J, Gros-louis F, Caroni P (2013)
791 Neuroprotection through Excitability and mTOR Required in ALS Motoneurons to
792 Delay Disease and Extend Survival. Neuron 80:80–96.

793 Sekerli M, Del Negro CA, Lee RH, Butera RJ (2004) Estimating action potential
794 thresholds from neuronal time-series: new metrics and evaluation of
795 methodologies. IEEE Trans Biomed Eng 51:1665–1672.

796 Shoenfeld L, Westenbroek RE, Fisher E, Quinlan K a, Tysseling VM, Powers RK,
797 Heckman CJ, Binder MD (2014) Soma size and Cav1.3 channel expression in
798 vulnerable and resistant motoneuron populations of the SOD1G93A mouse model of
799 ALS. Physiol Rep 2:e12113 Available at:
800 http://physreports.physiology.org/content/2/8/e12113.abstract.

801 van Zundert B, Peuscher MH, Hynynen M, Chen A, Neve RL, Brown RH, Constantine-
802 Paton M, Bellingham MC (2008) Neonatal neuronal circuitry shows hyperexcitable
803 disturbance in a mouse model of the adult-onset neurodegenerative disease

amyotrophic lateral sclerosis. J Neurosci Off J Soc Neurosci 28:10864–10874 Available at: https://doi.org/10.1523/JNEUROSCI.1340-08.2008.

Virtanen P et al. (2020) SciPy 1.0: fundamental algorithms for scientific computing in Python. Nat Methods:1–12 Available at: https://www.nature.com/articles/s41592-019-0686-2 [Accessed March 1, 2020].

Waskom M et al. (2020) mwaskom/seaborn: v0.10.0 (January 2020). Zenodo. Available at: https://doi.org/10.5281/zenodo.3629446.

Wasserstein RL, Schirm AL, Lazar NA (2019) Moving to a World Beyond "p < 0.05." Am Stat 73:1–19 Available at: https://amstat.tandfonline.com/doi/full/10.1080/00031305.2019.1583913 [Accessed April 13, 2020].

Welch BL (1947) The generalisation of student's problems when several different population variances are involved. Biometrika 34:28–35.